The Astrophysical Journal, 897:46 (10pp), 2020 July 1 https://doi.org/10.3847/1538-4357/ab9402

Gravitational-wave Captures by Intermediate-mass Black Holes in Galactic Nuclei

Giacomo Fragione[1,2], Abraham Loeb[3], Kyle Kremer[1,2], and Frederic A. Rasio[1,2]
[1] Center for Interdisciplinary Exploration & Research in Astrophysics (CIERA), Evanston, IL 60202, USA
[2] Department of Physics & Astronomy, Northwestern University, Evanston, IL 60202, USA
[3] Astronomy Department, Harvard University, 60 Garden Street, Cambridge, MA 02138, USA
Received 2020 February 7; revised 2020 May 7; accepted 2020 May 18; published 2020 July 1

Abstract

Intermediate-mass black holes (IMBHs) have not been detected beyond any reasonable doubt, despite their potential role as massive seeds for quasars and sources of tidal disruption events, ultraluminous X-ray sources, dwarf galaxy feedback, and hypervelocity stars. Gravitational wave (GW) observations can help to find and confirm the existence of IMBHs. Current and upcoming detectors, such as LIGO, Virgo, KAGRA, LISA, ET, and DECIGO promise to identify the full range from stellar-mass to supermassive black holes. In this paper, we address the question of whether IMBHs can produce GWs in galactic nuclei. We consider the possibility that stellar black holes (SBHs) form bound systems and later coalesce with an IMBH through gravitational captures in the dense nucleus. We show that this mechanism is efficient for IMBH masses in the range $\sim 3\times10^3\,M_\odot$–$2\times10^4\,M_\odot$. We find that the typical distributions of peak frequencies and merger timescales depend mainly on the IMBH mass. In particular, the typical peak frequency is about 0.2 Hz, 0.1 Hz, 0.09 Hz, and 0.05 Hz for $M_{\rm IMBH}=5\times10^3\,M_\odot$, $8\times10^3\,M_\odot$, $1\times10^4\,M_\odot$, and $2\times10^4\,M_\odot$, respectively. Our results show that, at design sensitivity, both DECIGO and ET should be able to detect these IMBH–SBH mergers. Furthermore, most of the mergers will appear eccentric ($e\gtrsim0.1$), providing an indication of their dynamical origin.

Unified Astronomy Thesaurus concepts: Astrophysical black holes (98); Black hole physics (159); Intermediate-mass black holes (816); Galaxy kinematics (602); Galaxy dynamics (591); Stellar dynamics (1596); Galactic center (565); Galaxy nuclei (609); Gravitational wave astronomy (675); Gravitational wave detectors (676); Gravitational wave sources (677); Gravitational waves (678)

1. Introduction

The possible existence of intermediate-mass black holes (IMBHs) is one of the unsolved questions of modern astronomy (Mezcua 2017). IMBHs have masses in the range $\sim10^2\,M_\odot$ $M_\odot$ $10^5\,M_\odot$, higher than stellar black holes (SBHs) and lower than supermassive black holes (SMBH). While the latter two families have direct proof of their existence (Kormendy & Ho 2013; LIGO-Virgo Scientific Collaboration 2019b), there is only circumstantial observational evidence for IMBHs (Baldassare et al. 2018; Chilingarian et al. 2018; Lin et al. 2018). Owing to their potential role in a wide range of phenomena, including the origin of SMBH seeds and galaxy evolution (Madau & Rees 2001; Tagawa et al. 2020), tidal disruption events (Chen et al. 2011; Fragione & Leigh 2018b), gravitational-wave (GW) emission (Gair et al. 2011; Fragione & Leigh 2018a), ultraluminous X-ray binaries (Kaaret et al. 2017), such as HLX-1 in ESO243-49 (Farrell et al. 2009), dwarf galaxy feedback (Silk 2017), and hypervelocity stars (Yu & Tremaine 2003; Levin 2006; Rasskazov et al. 2019), finding observational imprints of the origin and evolution of IMBHs has recently attracted significant attention (see Greene et al. 2019 for a review).

There are at least three main pathways to form IMBHs. The first mechanism involves the collapse of massive Population III stars. Due to inefficient cooling, Population III stars of a few hundreds solar masses collapse to an IMBH of $\sim100\,M_\odot$ (Fryer et al. 2001; Madau & Rees 2001; Bromm & Larson 2004; Bromm 2013; Loeb & Furlanetto 2013). The second channel predicts that an IMBH of a very high mass ($\sim10^4$–$10^6\,M_\odot$) may be born following the collapse of a gas clouds without passing through all the phases of stellar evolution (Loeb & Rasio 1994; Bromm & Loeb 2003; Begelman et al. 2006). IMBHs with masses in between these two extremes can be produced through gravitational runaway events in star clusters (Portegies Zwart & McMillan 2002; Giersz et al. 2015). In this contest, repeated mergers of massive stars (Gürkan et al. 2004; Freitag et al. 2006; Pan et al. 2012) or SBHs (Miller & Hamilton 2002; Antonini & Rasio 2016) can give birth to an IMBH with mass $\sim10^3$–$10^4\,M_\odot$. Other possibilities include the fragmentation of SMBH accretion disks (McKernan et al. 2012, 2014) and super-Eddington accretion onto SBHs in SMBH accretion disks (Kocsis et al. 2011).

Recent efforts have been directed toward understanding all the possible observational imprints of IMBHs, which could be detected in a number of different ways. Accreting IMBHs could be found from radio to X-ray in galactic nuclei (Greene & Ho 2007; Baldassare et al. 2018; Chilingarian et al. 2018) or as ultraluminous X-ray sources in the field (Kaaret et al. 2017). The presence of dormant IMBHs can be inferred from stellar and gas dynamical searches both in galactic nuclei and globular clusters (Gualandris et al. 2010; Baumgardt et al. 2019; Girma & Loeb 2019). In these environments, IMBHs can also disrupt stars, resulting in detectable tidal disruption events (Fragione & Leigh 2018b; Fragione et al. 2018b; Lin et al. 2018). The disruption of a white dwarf is of particular interest, as such an event is luminous only for IMBHs with masses $10^5\,M_\odot$, which have a Schwarzschild radius smaller than the white dwarf disruption radius (Rosswog et al. 2008, 2009; Peng et al. 2019; Shen 2019).

GW astronomy will help in the hunt for the first IMBHs to be discovered beyond any doubt (Konstantinidis et al. 2013; Arca-Sedda et al. 2019). IMBH–SBH binaries may form in the cores of star clusters or in galactic nuclei, and may merge as intermediate-mass-ratio inspirals (IMRIs; Amaro-Seoane et al. 2007; Mandel et al. 2008; Fragione et al. 2018b). Present and

upcoming GW observatories, including LIGO,[4] the Einstein Telescope[5] (ET), and LISA,[6] will be able to detect GW sources from IMBHs of masses up to ~ 100–$1000\,M_\odot$, $\sim 10^3$–$10^4\,M_\odot$ and $10^4\,M_\odot$, respectively (Bellovary et al. 2019). Another third-generation mission, DECIGO,[7] could reveal GW events across most of the IMBH mass spectrum. Using the nondetection of massive binaries in the first two observational runs, the LIGO/Virgo collaboration placed upper limits on merging IMBHs, of the order of ~ 0.1–$1\ \mathrm{Gpc^{-3}\ yr^{-1}}$ (LIGO/Virgo Scientific Collaboration 2019a).

Here we address the question of whether IMBHs can produce observable GW sources in galactic nuclei. Specifically, we consider the possibility that SBHs form a binary with an IMBH as a result of gravitational bremsstrahlung, with the binary later merging as an IMRI. While this process has been widely discussed in the context of SBH–SBH captures in galactic nuclei and star clusters (O'Leary et al. 2009; Gondán et al. 2018; Rasskazov & Kocsis 2019; Samsing et al. 2019), the IMBH regime has received less attention.

The paper is organized as follows. In Section 2, we discuss how IMBHs form and migrate in galactic nuclei. In Section 3, we discuss the process of capture through gravitational bremsstrahlung. In Section 4, we describe our Monte Carlo framework, and we derive the typical GW signals as a function of GW peak frequency and GW strain in Section 5. We estimate the IMBH–SBH merger rates from this process in Section 6. Finally, we discuss the implications of our findings and draw our conclusions in Section 7.

2. Intermediate-mass Black Holes in Galactic Nuclei

Several mechanisms exist that could create IMBHs in galactic nuclei. They can either form ex situ or in situ. In the former case, IMBHs have to be delivered to the innermost galactic regions by some dissipation mechanism. Below, we describe some of these scenarios in more detail.

Star clusters are promising environments for forming an IMBH. This would be natural, assuming that the observed relation between SMBH mass and the velocity dispersion of stars around it holds also for IMBHs (Merritt 2013). A number of studies showed that the most massive stars may segregate and merge in the core of the cluster, forming a massive growing object that can later collapse to an IMBH (Portegies Zwart & McMillan 2002; Gürkan et al. 2004; Freitag et al. 2006; Giersz et al. 2015). In this case, the typical IMBH mass would be in the range $\sim 10^3$–$10^4\,M_\odot$. Star clusters born in the innermost galactic regions could inspiral into the centers of galaxies by dynamical friction on timescales much shorter than a Hubble time (Tremaine et al. 1975; Capuzzo-Dolcetta & Miocchi 2008; Gnedin et al. 2014). If these GCs host central IMBHs, this process could efficiently deliver these IMBHs to galactic centers (Gürkan & Rasio 2005; Mastrobuono-Battisti et al. 2014; Arca-Sedda & Gualandris 2018; Fragione et al. 2018a). In this scenario, the IMBH forms ex situ, and is delivered to the galactic nucleus by dynamical friction acting on his parent cluster.

A second ex situ formation scenario for IMBH is due to minor mergers of galaxies (Volonteri et al. 2003). Following the mergers of galaxies, IMBHs can be delivered to the proximity of the major galaxy nucleus, owing to three different processes (Merritt & Milosavljević 2005). First, the IMBH inspirals independently toward the center of the gravitational potential via dynamical friction. This is followed by a stage where the system loses energy, and angular momentum as a result of stellar gravitational slingshots (Quinlan 1996; Sesana et al. 2006; Rasskazov et al. 2019). This process eventually drives the system to the subsequent stage of energy loss, due to emission of GWs (Merritt & Milosavljević 2005; Dosopoulou & Antonini 2017). In this scenario, the IMBH is formed in a larger environment than a star cluster, as within a dwarf galaxy (Silk 2017; Chilingarian et al. 2018), and its mass would typically be in the range $\sim 10^3$–$10^5\,M_\odot$.

Another mechanism that produces and delivers IMBHs close to the galactic nucleus involves Population III stars. In this scenario, IMBHs form as the remnants of the very first massive stars (Volonteri et al. 2008; Volonteri & Natarajan 2009), while dynamical friction would then deliver some of them close to the SMBH within a Hubble time (Madau & Rees 2001). In this channel, the typical IMBH mass would be $\sim 10^2$–$10^3\,M_\odot$, but significant accretion could later increase it significantly.

A different formation scenario is that of a collapsing gas cloud, which forms a massive IMBH without passing through the phases of stellar evolution (Loeb & Rasio 1994; Bromm & Loeb 2003). This channel produces IMBHs of $\sim 10^4$–$10^6\,M_\odot$, but could only work at high redshifts, where the pristine gas can efficiently suppress cooling and fragmentation.

IMBHs could also form efficiently in situ in the gaseous disks of active galactic nuclei (AGNs; McKernan et al. 2012, 2014). If migration traps are present in the gaseous disk surrounding an SMBH, differential gas torques exerted on the orbiting SBHs will cause them to migrate toward a migration trap (Secunda et al. 2019). Turbulence in the gaseous disk can knock orbiting SBHs out of resonance, but it allows them to drift close to the trap and experience a close interaction with the first SBH. The interactions are dissipative due to the gas, and it is possible that SBH–SBH binaries form and merge repeatedly, thus forming an IMBH (Yang et al. 2019; McKernan et al. 2020). The masses of the IMBHs are poorly constrained in this scenario, and IMBHs could continue to accrete gas, thus increasing their masses considerably (McKernan et al. 2014).

If a gaseous disk is not present, IMBHs can form though repeated mergers of SBHs in dense systems (Antonini & Rasio 2016). Here, the requirement is that the host nuclear cluster is dense and massive enough to retain the merger remnant following its recoil kick due to asymmetric emission of GWs (Lousto & Zlochower 2008; Lousto et al. 2012; Hofmann et al. 2016). If the merger products are retained, they can form dynamically new binaries with SBHs and merge again, thus leading to a significant mass growth (Antonini et al. 2019). The typical IMBH mass would be $\sim 10^2$–$10^4\,M_\odot$.

3. Gravitational Bremsstrahlung

We start by deriving the cross sections for IMBH bremsstrahlung in galactic nuclei.

We first consider the cross section for an IMBH of mass, $M_{\rm IMBH}$, to undergo an encounter with an SBH of mass $m_2 = qM_{\rm IMBH}$ ($M_{\rm IMBH} > m_2$), within a pericenter distance r_p $_{\rm cap}$. We define $_{\rm cap}$ to be the maximum distance below which $M_{\rm IMBH}$ and m_2 remain bound. In the gravitational focusing limit, the

[4] http://www.ligo.org
[5] http://www.et-gw.eu
[6] https://lisa.nasa.gov
[7] http://tamago.mtk.nao.ac.jp/decigo/index_E.html

encounter cross section is simply (Quinlan & Shapiro 1987)

$$s_{\rm cap} = 2\pi G \frac{M_{\rm IMBH}(1+q)}{v^2} {}_{\rm cap}, \quad (1)$$

where $v \sim (GM_{\rm SMBH}/r)^{1/2}$ (r is the distance from the SMBH) is the local dispersion velocity. For an interaction to result in a GW capture, the energy radiated at the first pericenter passage from GW emission (Turner 1977),

$$\Delta E_{\rm GW} = \frac{85\pi}{12\sqrt{2}} \frac{G^{7/2}}{c^5} \frac{M_{\rm IMBH}^{9/2}}{{}_{\rm cap}^{7/2}} q^2 (1+q)^{1/2}, \quad (2)$$

has to be equal to the relative kinetic energy $(1/2)\mu v^2$, where μ is the reduced mass of the binary,

$$\mu = M_{\rm IMBH} \frac{q}{1+q}. \quad (3)$$

This fixes the maximum pericenter distance ${}_{\rm cap}$ to

$$\begin{aligned} {}_{\rm cap} &= R_{\rm S,1} \left(\frac{85\pi}{96}\right)^{2/7} \left(\frac{c}{v}\right)^{4/7} q^{2/7} (1+q)^{3/7} \\ &= R_{\rm S,1} \left(\frac{85\pi}{96}\right)^{2/7} \left(\frac{c}{v_h}\right)^{4/7} \left(\frac{r}{r_h}\right)^{2/7} q^{2/7} (1+q)^{3/7}, \end{aligned} \quad (4)$$

where $R_{\rm S,1} = 2GM_{\rm IMBH}/c^2$ is the Schwarzschild radius of the IMBH. The semimajor axis and eccentricity of the new-formed binary can be derived as (O'Leary et al. 2009)

$$a = \frac{GM_{\rm IMBH}^2 q}{2|E_F|} \quad (5)$$

and

$$e = \left(1 - \frac{2|E_F| v^2 b^2}{G^2 M_{\rm IMBH}^3 q (1+q)}\right)^{1/2}, \quad (6)$$

respectively. In the previous equations, $E_F = \frac{1}{2}\mu v^2 - \Delta E_{\rm GW}$, and b is the impact parameter, related to the pericenter of the orbit through (assuming gravitational focusing),

$$r_p \approx \frac{b^2 v^2}{2GM_{\rm IMBH}(1+q)}. \quad (7)$$

Therefore, the maximum impact parameter for a bremsstrahlung capture is for $r_p = {}_{\rm cap}$,

$$b_{\rm max} \approx \frac{[2G\ {}_{\rm cap} M_{\rm IMBH}(1+q)]^{1/2}}{v}. \quad (8)$$

Requiring a minimum pericenter to avoid head-on collisions sets the limit for the minimum impact parameter (Gondán et al. 2018),

$$b_{\rm min} = \frac{4GM_{\rm IMBH}(1+q)}{cv}. \quad (9)$$

The peak frequency at formation is (Wen 2003)

$$f_{\rm GW} = \frac{\sqrt{GM_{\rm IMBH}(1+q)}}{\pi} \frac{(1+e)^{1.1954}}{[a(1-e^2)]^{1.5}}. \quad (10)$$

After the binary is formed, it evolves, due to GW radiation reaction, and merges on a timescale (Peters 1964)

$$T_{\rm GW,IMBHB} = \frac{5}{256} \frac{a^4 c^5}{G^3 M_{\rm IMBH}^3 q(1+q)} (1-e^2)^{7/2}. \quad (11)$$

To derive the relevant timescales, we need to quantify the stellar and compact-object populations within the SMBH sphere of influence. The sphere of influence is defined as the region within the characteristic radius (Merritt 2013),

$$r_h = \frac{GM_{\rm SMBH}}{v_h^2}, \quad (12)$$

where v_h is the galactic dispersion velocity at the radius of influence. A number of studies have found that stars and compact objects form cuspy profiles (Bahcall & Wolf 1976; Hopman & Alexander 2006; Perets et al. 2007; Aharon & Perets 2015; Fragione & Sari 2018). For simplicity, we assume that the cusp is dominated by solar-mass stars, with density profile (O'Leary et al. 2009; Amaro-Seoane & Preto 2011),

$$n_{\rm MS} = \frac{N_{\rm MS}}{A r_h^3} \left(\frac{r}{r_h}\right)^{-\alpha_{\rm MS}}, \quad (13)$$

where $A = 4\pi/3$, $\alpha_{\rm MS} \sim 1.6$, and $N_{\rm MS}$ is the number of objects at the influence radius given by (see Equation (9) in Gondán et al. 2018),

$$n_{\rm MS}(r = r_h) = \frac{N_{\rm MS}}{A r_h^3} = 1.4 \times 10^5\ {\rm pc}^{-3} \left(\frac{10^6\ M_\odot}{M_{\rm SMBH}}\right)^{1/2}. \quad (14)$$

The effect of different SMBH masses has been accounted for through the "M-σ" relation (Tremaine et al. 2002),

$$M_{\rm SMBH} = \eta v_h^4, \quad (15)$$

where $\eta = 4 \times 10^{-2}\ M_\odot\ ({\rm km\ s^{-1}})^{-4}$ is a constant, and v_h is the velocity dispersion at the influence radius r_h of the SMBH. Using this M-σ relation, r_h and T_h can be rewritten as

$$r_h = G\eta^{1/2} M_{\rm SMBH}^{1/2}, \quad (16)$$

and

$$T_h = \frac{r_h}{v_h} = G\eta^{3/4} M_{\rm SMBH}^{1/4}, \quad (17)$$

respectively. We also consider an SBH population,

$$n_{\rm SBH} = \frac{N_{\rm SBH}}{A r_h^3} \left(\frac{r}{r_h}\right)^{-\alpha_{\rm BH}}, \quad (18)$$

where $N_{\rm SBH} = 0.023(3-\alpha_{\rm BH})/(3-\alpha_{\rm MS}) N_{\rm MS}$ (Gondán et al. 2018) and $\alpha_{\rm SBH} \sim 2$ (Bahcall & Wolf 1977; Hopman & Alexander 2006).[8]

Using Equations (1), (4), and (18), we can estimate the typical timescale (per IMBH) for the formation of an IMBH–SBH binary at a given position within the cusp,

$$T_{\rm IMBHB} = \frac{1}{n_{\rm SBH} s_{\rm cap} v}, \quad (19)$$

[8] For a mass spectrum, the characteristic slope of the cusp of a given population depends on the mass of the object; the more massive, the steeper it is (Keshet et al. 2009; Alexander 2017).

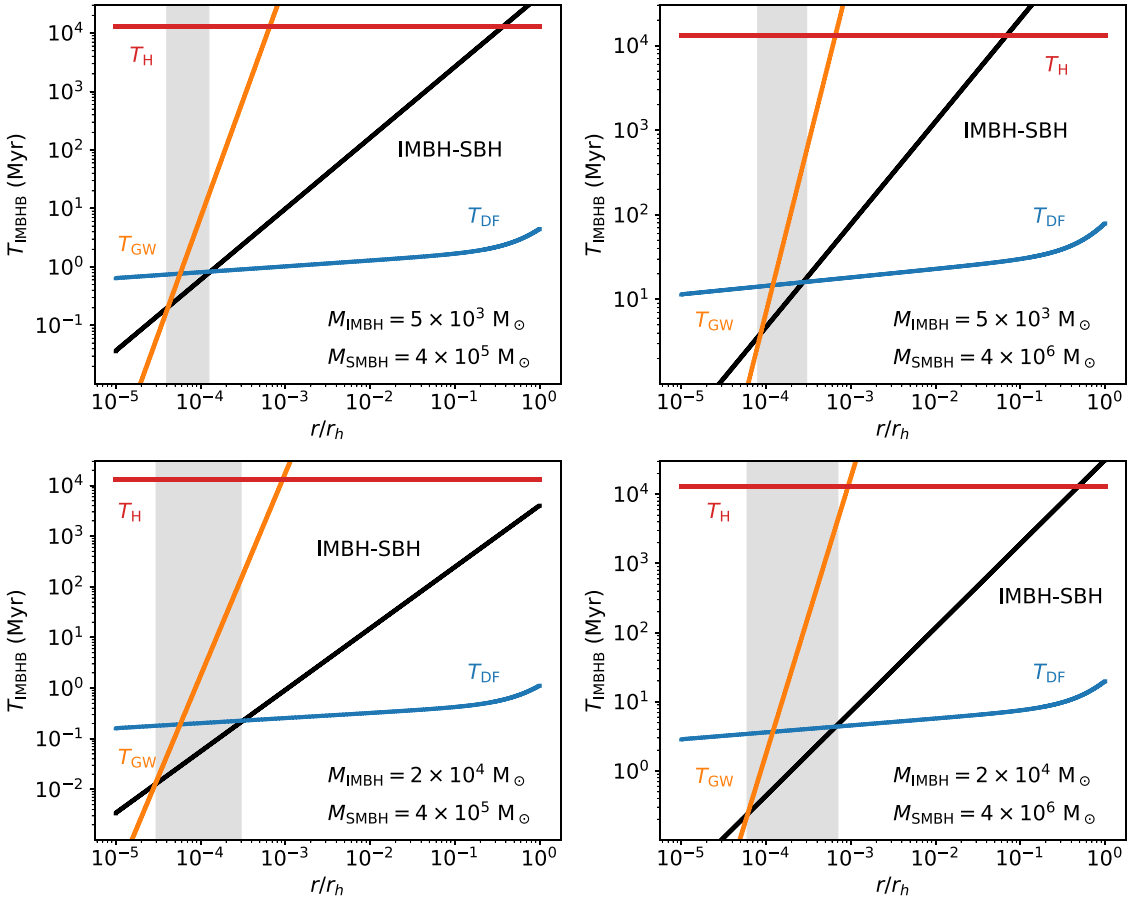

Figure 1. Typical timescale (per IMBH) for the formation of IMBH–SBH binaries (Equation (37)) at a given position within the cusp, for different IMBH masses. Left: $M_{\rm SMBH} = 4 \times 10^5\,M$; right: $M_{\rm SMBH} = 4 \times 10^6\,M$. Shown in the figure also the dynamical friction timescale (blue line), the GW merger timescale for the SMBH–IMBH system (orange line), and Hubble time (red line). The shaded region represents the available portion of the phase space where IMBH–SBH binaries can efficiently form and eventually merge.

where $n_{\rm SBH}$ is the number density of SBHs. Plugging the relevant parameters derived above, the typical timescale for the formation of a binary containing an IMBH can be rewritten as

$$T_{\rm IMBHB} = \frac{QA}{2\pi N_{\rm SBH}} T_h \frac{r_h}{r_{\rm cap}} \left(\frac{r}{r_h}\right)^{a_{\rm SBH}-1/2}, \qquad (20)$$

where $T_h = r_h/v_h$ is the orbital period at the influence radius, and $Q = M_{\rm SMBH}/(M_{\rm IMBH} + m_2)$.

An IMBH can capture SBHs whenever its inspiral time due to dynamical friction is long enough (Binney & Tremaine 1987). We estimate the dynamical friction timescale following Gürkan & Rasio (2005),

$$T_{\rm DF} = \frac{[1 + (4-a)/(6-a)z]\,(1+z)^{1/2} Q T_h}{(3-a)Bz} \left(\frac{r}{r_h}\right)^{3/2}. \qquad (21)$$

In the previous equation, $B \sim 1.7$ is a numerical factor of the order of unity that accounts for the dynamical friction coefficient and the Coulomb logarithm (McMillan & Portegies Zwart 2003), $a \sim 1.6$ is the overall cusp slope,[9] and $z(r) = M_{\rm cusp}(r)/M_{\rm SMBH}$ is the cusp mass at a given distance from the SMBH in units of the SMBH mass. At shorter distances, the inspiral is dominated by energy loss due to GW emission. In this case, an IMBH inspirals into the central SMBH on a timescale (Peters 1964),

$$T_{\rm GW} = \frac{5}{256} \frac{r_h^4 c^5}{G^3 M_{\rm IMBH}^3 Q(1+Q)} \left(\frac{r}{r_h}\right)^4 (1-e_{\rm IMBH}^2)^{7/2}, \qquad (22)$$

where $e_{\rm IMBH}$ is the IMBH orbital eccentricity.

In Figure 1, we show the typical timescale (per IMBH) for the formation of IMBH–SBH at a given position within the cusp for different IMBH and SMBH masses. As the distribution of SBHs is cuspy, the smallest bremsstrahlung timescale occurs at the smallest galactocentric distance. Far from the SMBH ($r/r_h \gtrsim 0.1$), the typical timescale to form binaries can exceed Hubble time. On the other hand, $T_{\rm IMBHB}$ becomes of the order of 10^{-1}–10^{1} Myr for smaller distances ($r/r_h \sim 10^{-3}$). The IMBH mass also affects the binary formation timescale. As $\sigma_{\rm cap} \propto M_{\rm IMBH}$ $_{\rm cap}$ (Equation (1)) and $_{\rm cap} \propto M_{\rm IMBH}^{5/7}$ (Equation (4)), $T_{\rm IMBHB} \propto M_{\rm IMBH}^{-12/7}$. As a consequence, the bremsstrahlung timescale for a $5 \times 10^3\,M$ IMBH is $\sim$10 times longer than for a $2 \times 10^4\,M$ IMBH. Moreover, $T_{\rm IMBHB} \propto M_{\rm SMBH}$, thus larger SMBH masses imply larger binary formation timescales.

We also report in Figure 1 the inspiral time due to dynamical friction and the GW merger timescale for the SMBH–IMBH

[9] Alexander & Hopman (2009) have shown that in the case of strong mass segregation, the dominant cusp of $1\,M$ stars would be distributed in a cusp with slope $\sim$1.4, while white dwarfs, neutron stars, and SBHs would be in cusp profiles with slopes $\sim$1.4, $\sim$1.5, and $\sim$2, respectively. In this case, the DF timescale would be even larger, due to the small number of stars that move slower than the IMBH (Antonini & Merritt 2012).

system (assuming $e_{\rm IMBH} \sim 0$).[10] An IMBH can capture SBHs whenever

$$T_{\rm IMBHB} < \min(T_{\rm DF}, T_{\rm GW}). \quad (23)$$

For large orbital separations of the IMBH with respect to the central SMBH, dynamical friction is the main mechanism to lose energy, while GW energy loss operates on smaller distances. The typical distance $r_{\rm peak}$ at which $T_{\rm DF} = T_{\rm GW}$ is independent on the IMBH mass, as both $T_{\rm DF}$ and $T_{\rm GW}$ are $\propto 1/M_{\rm IMBH}$. On the other hand, their slope depends on the SMBH mass and (for $T_{\rm DF}$) the cusp profile. The region where $T_{\rm IMBHB}$ is the smallest timescale corresponds to the available region of the phase space where IMBH–SBH binaries can efficiently form and eventually merge (shaded region in Figure 1). Actually, if an IMBH–SBH binary forms and $T_{\rm GW,IMBHB} > \max(T_{\rm DF}, T_{\rm GW})$, the IMBH–SBH will inspiral into the SMBH, producing a double LISA signal, essentially a superimposition of an IMRI (IMBH–SMBH inspiral) and an extreme-mass-ratio inspiral (EMRI; SBH–SMBH inspiral).

Figure 1 illustrates the allowed parameter space for forming IMBH–SBH binaries, for $M_{\rm IMBH} = 5 \times 10^3\,M_\odot$ (top) and $M_{\rm IMBH} = 2 \times 10^4\,M_\odot$ (bottom). Smaller IMBHs have longer dynamical friction and GW timescales, thus they will inspiral onto the SMBH on longer timescales. However, as $T_{\rm IMBHB} \propto M_{\rm IMBH}^{-12/7}$, it is less probable for smaller IMBHs to capture SBHs. As a result, the size of the available region depends importantly on the IMBH mass. We find that $T_{\rm IMBHB}$ is never the smallest timescale for $M_{\rm IMBH} \lesssim 3 \times 10^3\,M_\odot$. Heavier IMBHs can efficiently form binaries on short enough timescales. On the other hand, captured SBHs will typically have wide orbits, thus they are either orbitally unstable against SMBH perturbations (see Section 4) or could merge with the IMBH on timescales longer than its inspiral time. We find that this is almost always the case for masses $M_{\rm IMBH} \lesssim 2 \times 10^4\,M_\odot$.

In conclusion, gravitational bremsstrahlung is efficient in the IMBH mass range $3 \times 10^3\,M_\odot \lesssim M_{\rm IMBH} \lesssim 2 \times 10^4\,M_\odot$.

4. Monte Carlo Experiments

In this section, we describe the Monte Carlo framework we developed to derive the distributions of the relevant parameters of binaries formed through the GW capture of an SBH by an IMBH, including their GW peak frequencies and strains.

As an illustrative example, in the following we consider the bremsstrahlung by a single IMBH. We consider the IMBH mass in the range $[5 \times 10^3\,M_\odot - 2 \times 10^4\,M_\odot]$, and fix $m_2 = 10\,M_\odot$. Our Monte Carlo routine is based on the following steps:

1. We draw randomly the galactocentric location r in the interval $[r_{\rm min}; r_{\rm max}]$ where the bremsstrahlung takes place, by accounting for that the event $\propto \min(T_{\rm DF}, T_{\rm GW})/T_{\rm IMBHB}$. The minimum and maximum galactocentric distances are roots of the equations $T_{\rm IMBHB}(r_{\rm min}) = T_{\rm GW}(r_{\rm min})$ and $T_{\rm IMBHB}(r_{\rm max}) = T_{\rm DF}(r_{\rm max})$, respectively.

[10] This assumption is motivated by the fact that the initial inspiral is mostly governed by dynamical friction that operates to circularize the IMBH orbit.

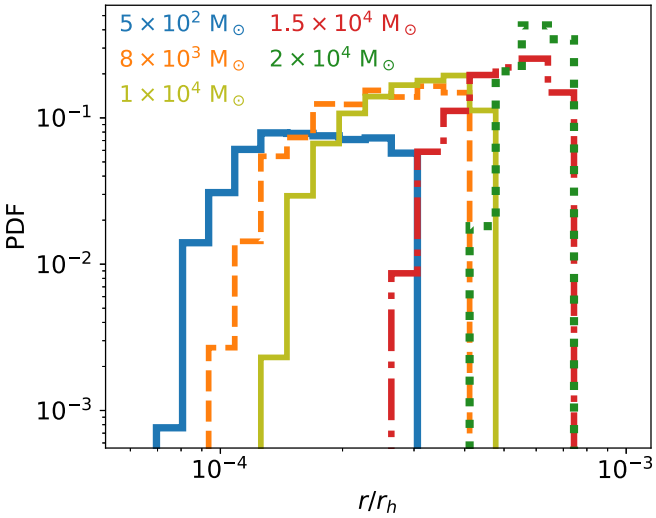

Figure 2. Distribution of galactocentric locations of the IMBH–SBH binaries formed from the GW capture of a $10\,M_\odot$ SBH, for different values of the IMBH mass. The mass of the SMBH is $M_{\rm SMBH} = 4 \times 10^6\,M_\odot$.

2. At a given galactocentric distance, we sample the relative velocity in the range $[0$–$v_{\rm max}(r)]$, where

$$v_{\rm max}(r) = \left(\frac{8GM_{\rm SMBH}}{r}\right)^{1/2}. \quad (24)$$

3. We compute the maximum pericenter that results in a capture $_{\rm cap}(r)$ from Equation (4).
4. We sample the impact parameter in the range $b_{\rm min}$–$b_{\rm max}$ (Equations (8)–(9)), with a distribution $f(b) \propto b$. In doing this, we note that $b_{\rm min} < b_{\rm max}$ can be violated for high values of the relative velocity (Gondán et al. 2018). This implies that these systems always suffer from a head-on collision.
5. We require that the binary is tidally stable against perturbations by the SMBH,

$$r \lesssim a\left(\frac{3M_{\rm SMBH}}{M_{\rm IMBH}}\right)^{1/3}, \quad (25)$$

where a is the binary semimajor axis.
6. We compute the semimajor axis (a), eccentricity (e), peak frequency ($f_{\rm GW}$), and GW merger timescale ($T_{\rm GW}$) of the newly formed binary.
7. The binary evolves according to (Peters 1964)

$$\frac{da}{dt} = -\frac{64}{5}\frac{G^3 M_{\rm IMBH} q(1+q)}{c^5 a^3 (1-e^2)^{7/2}}\left(1 + \frac{73}{24}e^2 + \frac{37}{96}e^4\right), \quad (26)$$

$$\frac{de}{dt} = -\frac{304}{15}\frac{G^3 M_{\rm IMBH} q(1+q)}{c^5 a^4 (1-e^2)^{5/2}}\left(e + \frac{121}{304}e^3\right), \quad (27)$$

and merges within $T_{\rm GW,IMBHB}$ (Equation (11)).

In Figure 2, we illustrate the distribution of galactocentric locations of the binaries formed from the GW capture of a $10\,M_\odot$ SBH for different values of the IMBH mass. The mass of the SMBH is $M_{\rm SMBH} = 4 \times 10^6\,M_\odot$. We find that the typical r/r_h of the IMBH–SBH depends on the IMBH mass. The smaller the IMBH mass, the closer to the SMBH the IMBH–SBH binary forms and merges. This behavior is the result of two effects. First, the region of the parameter space where $T_{\rm IMBHB} < \min(T_{\rm DF}, T_{\rm GW})$ is at smaller distances with respect to the SMBH for smaller IMBHs. Second, while

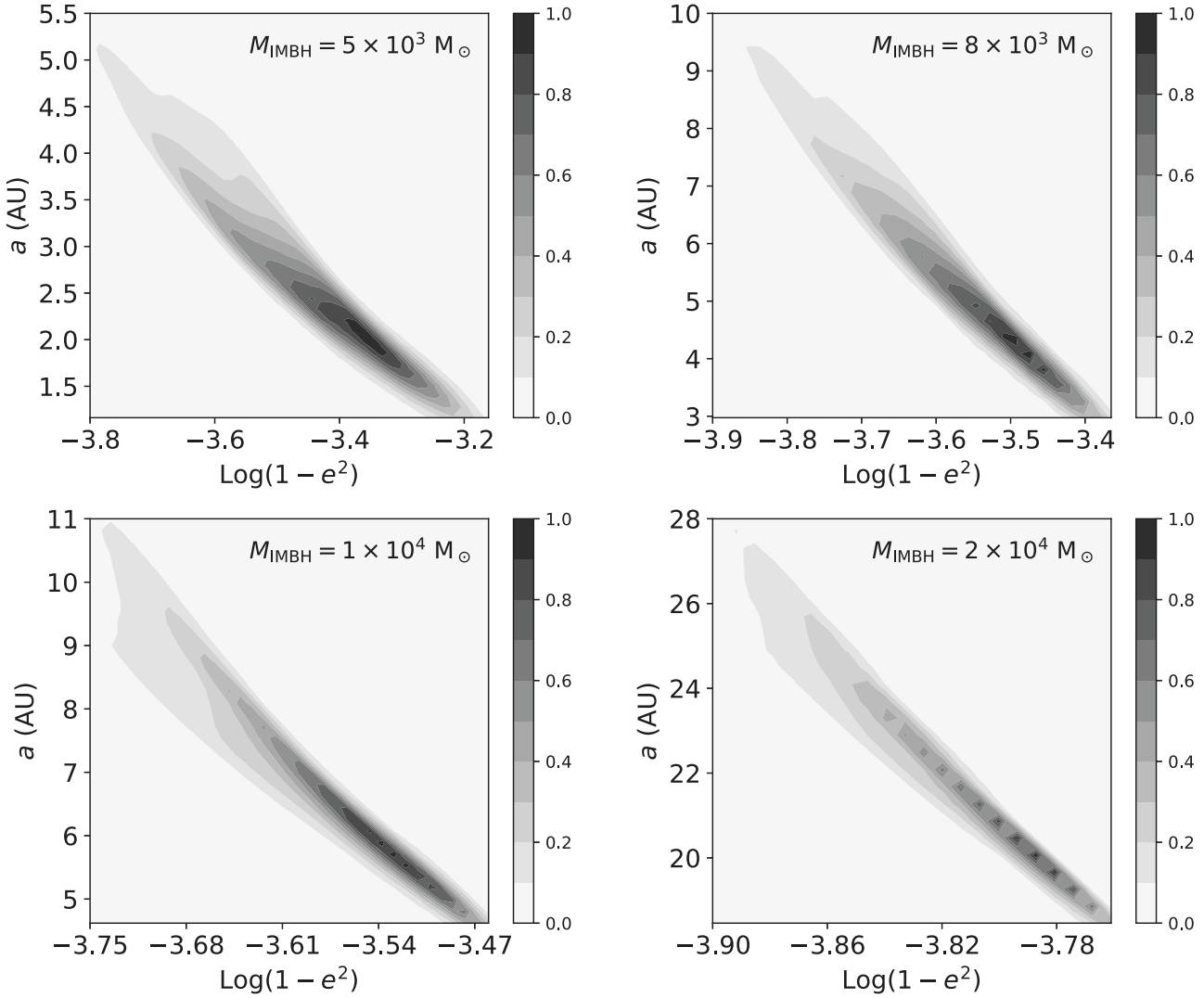

Figure 3. Distribution of semimajor axis a and $\epsilon = 1 - e^2$ of the IMBH–SBH of the binaries formed from the GW capture of a $10\,M_\odot$ SBH, for different values of the IMBH mass. The mass of the SMBH is $M_{\rm SMBH} = 4 \times 10^6\,M_\odot$. Color bar: normalized probability density.

heavier IMBHs can efficiently form binaries on short timescales in a wider area, captured SBHs will typically have wide orbits. As a result, they are either separated by the tidal field of the SMBH or inspiral into the IMBH on timescales longer than the IMBH inspiral time into the SMBH.

We show the distribution of semimajor axis a and $\epsilon = 1 - e^2$ of the IMBH–SBH, for $M_{\rm IMBH} = 5 \times 10^3\,M_\odot$, $8 \times 10^3\,M_\odot$, $1 \times 10^4\,M_\odot$, $2 \times 10^4\,M_\odot$, in Figure 3. For any IMBH mass, smaller IMBH–SBH semimajor axes imply less eccentric orbits. We find that the distribution of semimajor axis is peaked at $\sim$2 au, $\sim$5 au, $\sim$7 au, $\sim$20 au for $M_{\rm IMBH} = 5 \times 10^3\,M_\odot$, $8 \times 10^3\,M_\odot$, $1 \times 10^4\,M_\odot$, $2 \times 10^4\,M_\odot$, respectively, thus approximately $a \propto M_{\rm IMBH}^2$ (see also Equation (5)). On the other hand, the typical value of ϵ is smaller for larger IMBH masses. We find that the distribution of ϵ values is peaked at $\sim 4 \times 10^{-4}$, $\sim 3 \times 10^{-4}$, $\sim 2 \times 10^{-4}$, $\sim 1 \times 10^{-4}$ for $M_{\rm IMBH} = 5 \times 10^3\,M_\odot$, $8 \times 10^3\,M_\odot$, $1 \times 10^4\,M_\odot$, $2 \times 10^4\,M_\odot$, respectively. Thus, $\propto M_{\rm IMBH}^{-1}$ (see also Equation (6)).

In Figure 4, we illustrate the distribution of peak frequency and $T_{\rm GW,IMBHB}$, for $M_{\rm IMBH} = 5 \times 10^3\,M_\odot$, $8 \times 10^3\,M_\odot$, $1 \times 10^4\,M_\odot$, $2 \times 10^4\,M_\odot$. Different IMBH masses emit at different GW peak frequencies; the larger the IMBH mass, the smaller the $f_{\rm GW}$. In particular, we find a peak at $f_{\rm GW} \sim 0.2$ Hz, 0.1 Hz, 0.0.9 Hz, 0.05 Hz for $M_{\rm IMBH} = 5 \times 10^3\,M_\odot$, $8 \times 10^3\,M_\odot$, $1 \times 10^4\,M_\odot$, $2 \times 10^4\,M_\odot$, respectively. The distribution of GW merger timescales is peaked at $\sim$0.3 yr, $\sim$1 yr, $\sim$2 yr, $\sim$10 yr for $M_{\rm IMBH} = 5 \times 10^3\,M_\odot$, $8 \times 10^3\,M_\odot$, $1 \times 10^4\,M_\odot$, $2 \times 10^4\,M_\odot$, never long enough for external secular perturbations to matter. Note that this can be explained by considering

$$T_{\rm GW,IMBHB} \propto \frac{a^{4\ 7/2}}{M_{\rm IMBH}^2} \propto M_{\rm IMBH}^{5/2}. \tag{28}$$

While for SBH GW captures $T_{\rm GW}$ is of the order of seconds (O'Leary et al. 2009), thus resulting in a rapid GW signal, the merger timescale is of the order of minutes up to years for the IMBH regime.

5. Multiband Gravitational-wave Observations

We are now in the position to describe the typical GW signal expected from binaries merging as a result of the IMBH bremsstrahlung process.

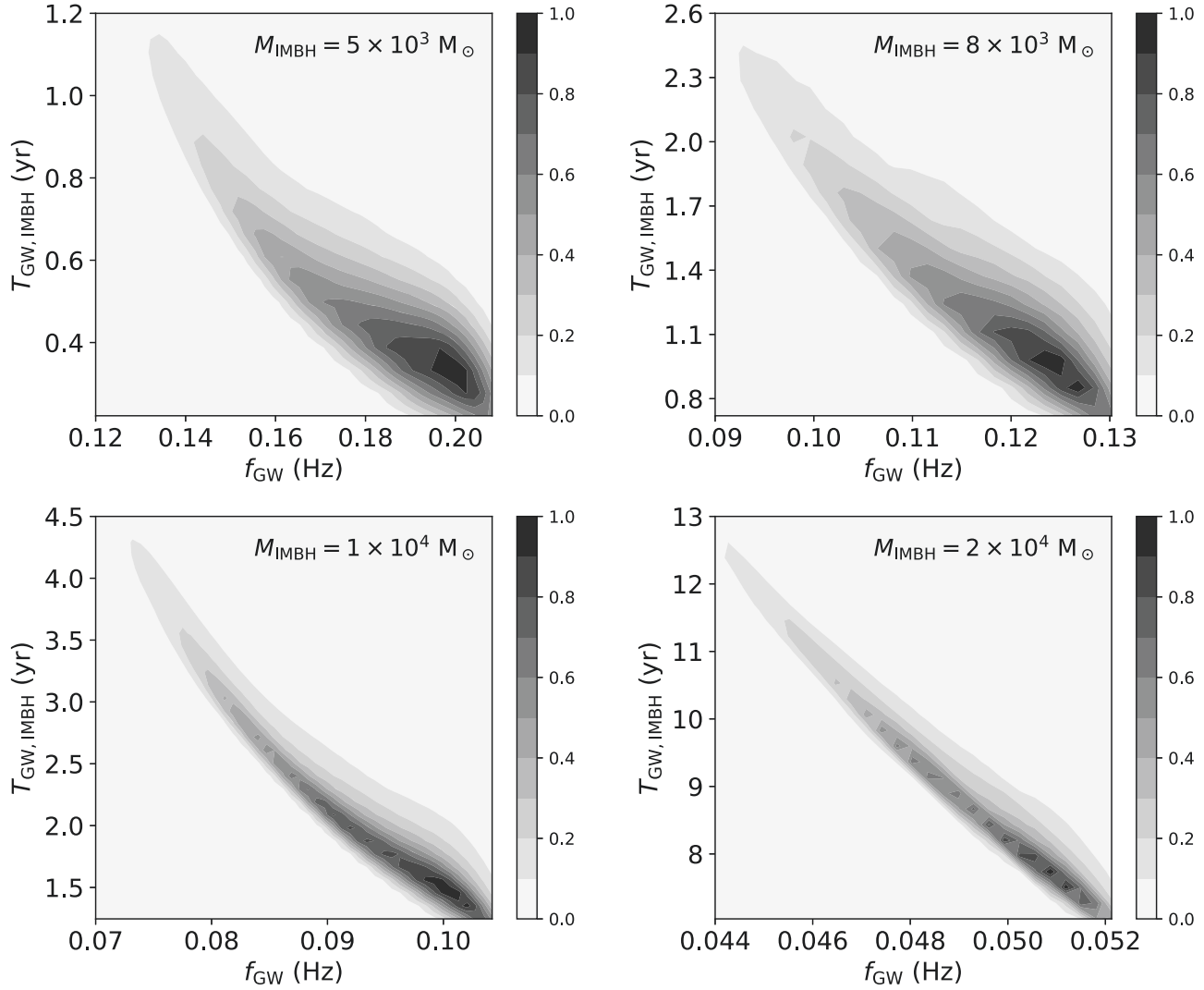

Figure 4. Distribution of peak frequency and GW merger timescale of the binaries formed from the GW capture of a $10\,M_\odot$ SBH, for different values of the IMBH mass. The mass of the SMBH is $M_{\rm SMBH} = 4 \times 10^6\,M_\odot$. Color bar: normalized probability density.

For an eccentric binary, the characteristic strain at the nth harmonic can be written as (Barack & Cutler 2004)

$$h_{\rm c,n}^2 = \frac{1}{(\pi D)^2}\left(\frac{2G}{c^3}\frac{E_{\rm n}}{f_{\rm n}}\right), \tag{29}$$

where

$$f_{\rm n} = n f_{\rm orb}, \tag{30}$$

where $f_{\rm orb}$ is the orbital frequency. This is related to the observed (detector frame) frequency $f_{\rm n,z}$ by $f_{\rm n} = f_{\rm n,z}(1+z)$. In Equation (29), $E_{\rm n}$ is the time derivative of the energy radiated by GWs at the frequency $f_{\rm n}$ (Peters & Mathews 1963),

$$E_{\rm n} = \frac{32}{5}\frac{G^{7/3}}{c^5}(2\pi f_{\rm orb})^{10/3} g(n,e), \tag{31}$$

where $M_{\rm c}$ is the rest-frame chirp mass,

$$M_{\rm c} = M_{\rm c,z}(1+z) = M_{\rm IMBH}\frac{q^{3/5}}{(1+q)^{1/5}}(1+z) \tag{32}$$

and $g(n,e)$ is a combination of Bessel functions of the first kind (see Equation (20) in Peters & Mathews 1963). Using $f_{\rm n} = n f_{\rm orb}$ and the semimajor axis Peters' equation (Peters 1964),

$$\frac{da}{dt} = -\frac{64}{5}\frac{G^3 M_{\rm IMBH}^3 q(1+q)}{c^5 a^3}F(e), \tag{33}$$

the derivative of the nth harmonic can be written as

$$f_{\rm n} = n\frac{96}{10\pi}\frac{(GM_{\rm c})^{5/3}}{c^5}(2\pi f_{\rm orb})^{11/3}F(e), \tag{34}$$

where

$$F(e) = \frac{1 + (73/24)e^2 + (37/96)e^4}{(1-e^2)^{7/2}}. \tag{35}$$

Combining Equations (31)–(34) and Equation (29), the characteristic strain at the nth harmonic can be rewritten as

$$h_{\rm c,n}^2 = \frac{2}{3\pi^{4/3}}\left(\frac{2}{n}\right)^{2/3}\frac{G^{5/3}M_{\rm c}^{5/3}}{f_{\rm n,z}^{1/3}(1+z)^2 c^3 D^2}\frac{g(n,e)}{F(e)}. \tag{36}$$

In the top panel of Figure 5, we show the evolution of the characteristic strain at frequency of peak emission for different values of the IMBH mass, assuming a distance of 250 Mpc

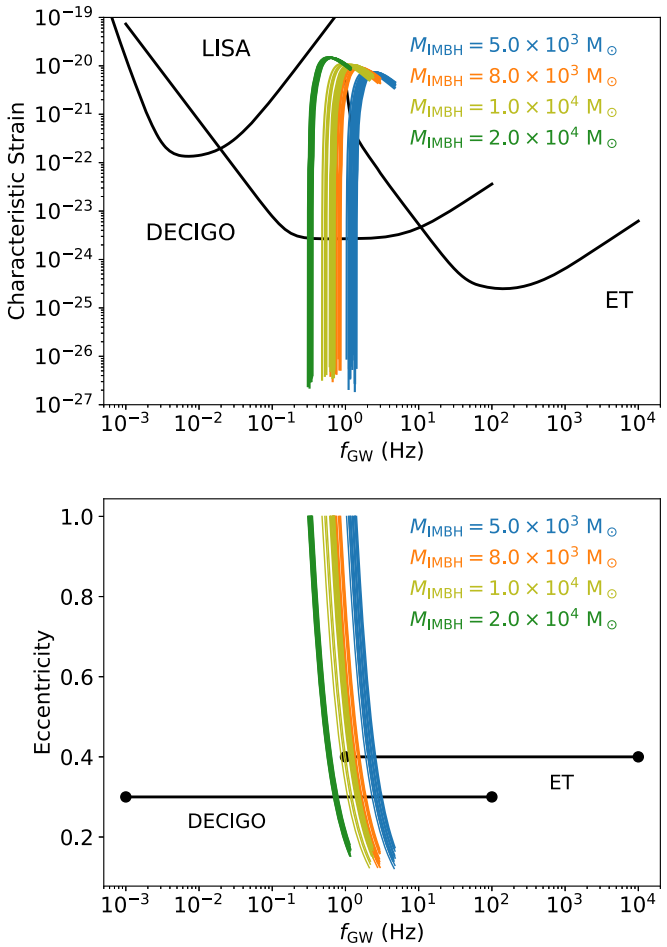

Figure 5. Evolution of the characteristic strain (top) and eccentricity (bottom) at frequency of peak emission for different values of the IMBH mass. We assume a distance of 250 Mpc from Earth. Black curves represent the ET (Hild et al. 2011), DECIGO (Yagi & Seto 2011), and LISA (Robson et al. 2019) sensitivity curves.

from Earth. We also show for comparison the sensitivity curves for ET (Hild et al. 2011), DECIGO (Yagi & Seto 2011), and LISA (Robson et al. 2019). Because we find that the typical peak frequency is ~0.2 Hz, 0.1 Hz, 0.09 Hz, 0.05 Hz for $M_{\rm IMBH} = 5 \times 10^3\,M$, $8 \times 10^3\,M$, $1 \times 10^4\,M$, $2 \times 10^4\,M$, respectively, merging IMBH of different masses will appear in the sensitivity frequency band of different instruments. Low-mass IMBHs typically will first appear in the DECIGO band, and than will be observed also by ET as they inspiral toward the merger. More massive IMBHs ($10^4\,M$) will appear only in DECIGO.

We illustrate the eccentricity evolution at frequency of peak emission in the bottom panel of Figure 5. We also plot the frequency range at which ET and DECIGO can measure IMBH–SBH inspirals. Some of the mergers still retain a nonnegligible eccentricity when they enter the detector frequency band, which will be typically 0.1. Measuring the retained eccentricity, using eccentric waveform templates, in particular when the inspiral can be detected by different instruments, would shed light on the formation scenario and reveal binaries formed as a result of gravitational bremsstrahlung in galactic nuclei. This holds true for IMBH binaries formed in the center of globular clusters (Mandel et al. 2008).

6. Rates

Next, we provide a simple estimate of the expected rate of GW events from IMBH bremsstrahlung.

The predominant population of IMBH–SBH binaries is formed at a typical distance ($r_{\rm peak}$) from the SMBH where the GW or dynamical friction timescale is the longest and $T_{\rm IMBHB}$ is the shortest. Therefore, typical number $N_{\rm IMBHB}$ of formed IMBH–SBH through captures is

$$N_{\rm IMBHB} \sim \max_{r_{\rm min} < \ll r_{\rm max}} \frac{\min(T_{\rm DF}, T_{\rm GW})}{T_{\rm IMBHB}} \sim \frac{T_{\rm GW}(r_{\rm peak})}{T_{\rm IMBHB}(r_{\rm peak})}, \quad (37)$$

where $r_{\rm peak}$ is the distance at which $T_{\rm DF}(r_{\rm peak}) = T_{\rm GW}(r_{\rm peak})$. From Figure 1, $N_{\rm IMBHB} \sim$ 3–5 over a timescale $T_{\rm GW}(r_{\rm peak}) \sim$ 10–15 yr for a $5 \times 10^3\,M$ IMBH in a Milky Way-like nucleus. For a $2 \times 10^4\,M$ IMBH, $N_{\rm IMBHB} \sim$ 6–10. Therefore, the rate of IMBH–SBH mergers can be as high as $\sim$ few $\rm yr^{-1}$ during the SMBH–IMBH inspiral.

The above numbers have been derived per IMBH hosted in a given nucleus at a given time. Of course, IMBHs can inspiral onto the SMBH, due to the combined effect of dynamical friction (Equation (21)) and GW emission (Equation (22)) producing a GW signal observable by LISA up to large redshifts (Arca-Sedda & Gualandris 2018). Eventually, the formation rate $\Gamma_{\rm form}$ of IMBHs (through the processes described in Section 2) would be large enough to replenish the innermost galactic regions with newly formed IMBHs. The Milky Way Galactic center may host several IMBHs in its nuclear star cluster, whose dynamical effects and/or nHz-frequency GW may be detected in the future. These considerations, along with constrains from the orbital stability of S-stars (Gualandris & Merritt 2009; Naoz et al. 2020) and proper motion measurements of Sgr A* (Hansen & Milosavljević 2003; Reid & Brunthaler 2004), have been used to constrain the possible IMBH companion to the SMBH in our Galactic center within the central parsec. Interestingly, the relevant range of IMBH masses for GW captures in a Milky Way-like nucleus overlaps with the allowed parameter space for a secondary massive black hole in our Galactic center. Therefore, monitoring Sgr A* with ET and DECIGO could place tighter constraints on the possible secondary IMBH, companion to Sgr A*.

If the formation rate is larger than the merging rate, $\Gamma_{\rm form} \gg 1/\min(T_{\rm DF}, T_{\rm GW})$, more than one IMBH can accumulate in a given galactic nucleus. In the calculation above, we have considered the bremsstrahlung process from a single IMBH. If more IMBHs are present within the SMBH sphere of influence, we could in principle apply the same procedure outlined above for all of them. In this case, it would be important to also compute the typical timescale for 2 IMBHs interacting, which could affect the rate estimate to some extent. Assuming a distribution of IMBHs as

$$n_{\rm IMBH} = \frac{N_{\rm IMBH}}{A r_h^3} \left(\frac{r}{r_h}\right)^{-a_{\rm IMBH}}, \quad (38)$$

where $N_{\rm IMBH}$ is the number of IMBHs, the IMBH–IMBH interaction timescale would be

$$T_{\rm 2IMBH} = \frac{1}{N_{\rm IMBH} n_{\rm IMBH} \Sigma_{\rm cap} v}. \quad (39)$$

Interestingly, this mechanism can create IMBH binaries, which can later merge and can possibly be kicked out by GW recoil kicks (O'Leary & Loeb 2012). We leave more detailed calculations of these effects to a future work.

7. Discussion and Conclusions

IMBHs are one of the unsolved puzzles of modern astronomy with no conclusive evidence for their existence. They attract much interest, owing to their important role in a wide range of phenomena, including the origin of SMBH seeds and galaxy evolution, tidal disruption events, dwarf galaxy feedback, and hypervelocity stars.

In this paper, we have described and outlined for the first time the characteristics of the GW sources produced through IMBH–SBH captures in galactic nuclei. We have shown that the typical semimajor axis, eccentricity, peak GW frequency, and merger timescales of the IMBH–SBH binaries formed as a result of this process depend mainly on the IMBH mass. In particular, we have found that the typical peak frequency is ∼0.2 Hz, 0.1 Hz, 0.09 Hz, 0.05 Hz for $M_{\rm IMBH} = 5 \times 10^3\,M_\odot$, $8 \times 10^3\,M_\odot$, $1 \times 10^4\,M_\odot$, $2 \times 10^4\,M_\odot$, respectively. As such, low-mass IMBHs will typically appear in both DECIGO and ET bands, while more massive IMBHs only in DECIGO as they merge. Interestingly, while the merger timescales is of the order of seconds for SBH GW captures (O'Leary et al. 2009), thus resulting in a rapid GW inspiral signal, it is of order months to years for the IMBH regime. Some of the mergers will appear eccentric in the detector frequency band.

As in the process described here for SBHs, IMBHs can also capture neutron stars, main-sequence stars, and white dwarfs. For white dwarfs, through the strong tidal interaction, this mechanism could trigger a thermonuclear explosion. The consumption of a white dwarf would be extremely interesting, as these events are luminous only for IMBH with masses $10^5\,M_\odot$ (Rosswog et al. 2008, 2009; MacLeod et al. 2016).

Finally, we note that a similar calculation can be done for IMBH gravitational bremsstrahlung outside the SMBH influence radius and in galactic nuclei that do not host SMBHs. The latter might be the case of galaxies with mass $10^9\,M_\odot$ (Ferrarese et al. 2006; Capuzzo-Dolcetta & Tosta e Melo 2017). The same exact process would be relevant in globular clusters hosting an IMBH in their center (Mandel et al. 2008).

By measuring the mass, spin, and redshift distributions for IMBH–SBH mergers, next-generation GW observations may help to improve our understanding of galaxy formation and galactic nuclei.

We thank the referee for a constructive report. G.F. acknowledges support from a CIERA Fellowship at Northwestern University. This work was supported in part by Harvard's black hole Initiative, which is funded by grants from JFT and GBMF. K.K., and F.A.R. acknowledge support from NSF grant AST-1716762.

ORCID iDs

Giacomo Fragione https://orcid.org/0000-0002-7330-027X
Abraham Loeb https://orcid.org/0000-0003-4330-287X
Kyle Kremer https://orcid.org/0000-0002-4086-3180
Frederic A. Rasio https://orcid.org/0000-0002-7132-418X

References

Aharon, D., & Perets, H. B. 2015, ApJ, 799, 185
Alexander, T. 2017, ARA&A, 55, 17
Alexander, T., & Hopman, C. 2009, ApJ, 697, 1861
Amaro-Seoane, P., Gair, J. R., Freitag, M., et al. 2007, CQGra, 24, R113
Amaro-Seoane, P., & Preto, M. 2011, CQGra, 28, 094017
Antonini, F., Gieles, M., & Gualandris, A. 2019, MNRAS, 486, 5008
Antonini, F., & Merritt, D. 2012, ApJ, 745, 83
Antonini, F., & Rasio, F. A. 2016, ApJ, 831, 187
Arca Sedda, M., Berry, C., Jani, K., et al. 2019, arXiv:1908.11375
Arca-Sedda, M., & Gualandris, A. 2018, MNRAS, 477, 4423
Bahcall, J. N., & Wolf, R. A. 1976, ApJ, 209, 214
Bahcall, J. N., & Wolf, R. A. 1977, ApJ, 216, 883
Baldassare, V. F., Geha, M., & Greene, J. 2018, ApJ, 868, 152
Barack, L., & Cutler, C. 2004, PhRvD, 70, 122002
Baumgardt, H., He, C., Sweet, S. M., et al. 2019, MNRAS, 488, 5340
Begelman, M. C., Volonteri, M., & Rees, M. J. 2006, MNRAS, 370, 289
Bellovary, J., Brooks, A., Colpi, M., et al. 2019, BAAS, 51, 175
Binney, J., & Tremaine, S. 1987, Galactic Dynamics (Princeton, NJ: Princeton Univ. Press)
Bromm, V. 2013, RPPh, 76, 112901
Bromm, V., & Larson, R. B. 2004, ARA&A, 42, 79
Bromm, V., & Loeb, A. 2003, ApJ, 596, 34
Capuzzo-Dolcetta, R., & Miocchi, P. 2008, MNRAS, 388, L69
Capuzzo-Dolcetta, R., & Tosta e Melo, I. 2017, MNRAS, 472, 4013
Chen, X., Sesana, A., Madau, P., & Liu, F. K. 2011, ApJ, 729, 13
Chilingarian, I. V., Katkov, I. Y., Zolotukhin, I. Y., et al. 2018, ApJ, 863, 1
Dosopoulou, F., & Antonini, F. 2017, ApJ, 840, 31
Farrell, S. A., Webb, N. A., Barret, D., Godet, O., & Rodrigues, J. M. 2009, Natur, 460, 73
Ferrarese, L., Côté, P., Dalla Bontà, E., et al. 2006, ApJL, 644, L21
Fragione, G., Ginsburg, I., & Kocsis, B. 2018a, ApJ, 856, 92
Fragione, G., & Leigh, N. 2018a, MNRAS, 480, 5160
Fragione, G., & Leigh, N. 2018b, MNRAS, 479, 3181
Fragione, G., Leigh, N. W. C., Ginsburg, I., & Kocsis, B. 2018b, ApJ, 867, 119
Fragione, G., & Sari, R. 2018, ApJ, 852, 51
Freitag, M., Gürkan, M. A., & Rasio, F. A. 2006, MNRAS, 368, 141
Fryer, C. L., Woosley, S. E., & Heger, A. 2001, ApJ, 550, 372
Gair, J. R., Mandel, I., Miller, M. C., & Volonteri, M. 2011, GReGr, 43, 485
Giersz, M., Leigh, N. W., Hypki, A., Lützgendorf, N., & Askar, A. 2015, MNRAS, 454, 3150
Girma, E., & Loeb, A. 2019, MNRAS, 482, 3669
Gnedin, O. Y., Ostriker, J. P., & Tremaine, S. 2014, ApJ, 785, 71
Gondán, L., Kocsis, B., Raffai, P., & Frei, Z. 2018, ApJ, 860, 5
Greene, J. E., & Ho, L. C. 2007, ApJ, 670, 92
Greene, J. E., Strader, J., & Ho, L. C. 2019, arXiv:1911.09678
Gualandris, A., Gillessen, S., & Merritt, D. 2010, MNRAS, 409, 1146
Gualandris, A., & Merritt, D. 2009, ApJ, 705, 361
Gürkan, M. A., Freitag, M., & Rasio, F. A. 2004, ApJ, 604, 632
Gürkan, M. A., & Rasio, F. A. 2005, ApJ, 628, 236
Hansen, B. M. S., & Milosavljević, M. 2003, ApJL, 593, L77
Hild, S., Abernathy, M., Acernese, F., et al. 2011, CQGra, 28, 094013
Hofmann, F., Barausse, E., & Rezzolla, L. 2016, ApJL, 825, L19
Hopman, C., & Alexander, T. 2006, ApJL, 645, L133
Kaaret, P., Feng, H., & Roberts, T. P. 2017, ARA&A, 55, 303
Keshet, U., Hopman, C., & Alexander, T. 2009, ApJL, 698, L64
Kocsis, B., Yunes, N., & Loeb, A. 2011, PhRvD, 84, 024032
Konstantinidis, S., Amaro-Seoane, P., & Kokkotas, K. D. 2013, A&A, 557, A135
Kormendy, J., & Ho, L. C. 2013, ARA&A, 51, 511
Levin, Y. 2006, ApJ, 653, 1203
LIGO/Virgo Scientific Collaboration 2019a, PhRvD, 100, 064064
LIGO-Virgo Scientific Collaboration 2019b, PhRvX, 9, 031040
Lin, D., Strader, J., Carrasco, E. R., et al. 2018, NatAs, 2, 656
Loeb, A., & Furlanetto, S. R. 2013, The First Galaxies in the Universe (Princeton, NJ: Princeton Univ. Press)
Loeb, A., & Rasio, F. A. 1994, ApJ, 432, 52
Lousto, C. O., & Zlochower, Y. 2008, PhRvD, 77, 044028
Lousto, C. O., Zlochower, Y., Dotti, M., & Volonteri, M. 2012, PhRvD, 85, 084015
MacLeod, M., Guillochon, J., Ramirez-Ruiz, E., Kasen, D., & Rosswog, S. 2016, ApJ, 819, 3
Madau, P., & Rees, M. J. 2001, ApJL, 551, L27
Mandel, I., Brown, D. A., Gair, J. R., & Miller, M. C. 2008, ApJ, 681, 1431
Mastrobuono-Battisti, A., Perets, H. B., & Loeb, A. 2014, ApJ, 796, 40
McKernan, B., Ford, K. E. S., Kocsis, B., Lyra, W., & Winter, L. M. 2014, MNRAS, 441, 900
McKernan, B., Ford, K. E. S., Lyra, W., & Perets, H. B. 2012, MNRAS, 425, 460

McKernan, B., Ford, K. E. S., O'Shaughnessy, R., & Wysocki, D. 2020, MNRAS, 494, 1203
McMillan, S. L. W., & Portegies Zwart, S. F. 2003, ApJ, 596, 314
Merritt, D. 2013, Dynamics and Evolution of Galactic Nuclei (Princeton, NJ: Princeton Univ. Press)
Merritt, D., & Milosavljević, M. 2005, LRR, 8, 8
Mezcua, M. 2017, IJMPD, 26, 1730021
Miller, M. C., & Hamilton, D. P. 2002, MNRAS, 330, 232
Naoz, S., Will, C. M., Ramirez-Ruiz, E., et al. 2020, ApJL, 888, L8
O'Leary, R. M., Kocsis, B., & Loeb, A. 2009, MNRAS, 395, 2127
O'Leary, R. M., & Loeb, A. 2012, MNRAS, 421, 2737
Pan, T., Loeb, A., & Kasen, D. 2012, MNRAS, 423, 2203
Peng, Z.-K., Yang, Y.-S., Shen, R.-F., et al. 2019, ApJL, 884, L34
Perets, H. B., Hopman, C., & Alexander, T. 2007, ApJ, 656, 709
Peters, P. C. 1964, PhRv, 136, 1224
Peters, P. C., & Mathews, J. 1963, PhRv, 131, 435
Portegies Zwart, S. F., & McMillan, S. L. W. 2002, ApJ, 576, 899
Quinlan, G. D. 1996, NewA, 1, 35
Quinlan, G. D., & Shapiro, S. L. 1987, ApJ, 321, 199
Rasskazov, A., Fragione, G., Leigh, N. W. C., et al. 2019, ApJ, 878, 17
Rasskazov, A., & Kocsis, B. 2019, ApJ, 881, 20
Reid, M. J., & Brunthaler, A. 2004, ApJ, 616, 872
Robson, T., Cornish, N. J., & Liu, C. 2019, CQGra, 36, 105011
Rosswog, S., Ramirez-Ruiz, E., & Hix, W. R. 2008, ApJ, 679, 1385
Rosswog, S., Ramirez-Ruiz, E., & Hix, W. R. 2009, ApJ, 695, 404
Samsing, J., D'Orazio, D. J., Kremer, K., Rodriguez, C. L., & Askar, A. 2019, arXiv:1907.11231
Secunda, B., Bellovary, J., Mac Low, M.-M., et al. 2019, ApJ, 878, 85
Sesana, A., Haardt, F., & Madau, P. 2006, ApJ, 651, 392
Shen, R.-F. 2019, ApJL, 871, L17
Silk, J. 2017, ApJL, 839, L13
Tagawa, H., Haiman, Z., & Kocsis, B. 2020, ApJ, 892, 36
Tremaine, S., Gebhardt, K., Bender, R., et al. 2002, ApJ, 574, 740
Tremaine, S. D., Ostriker, J. P., & Spitzer, L. J. 1975, ApJ, 196, 407
Turner, M. 1977, ApJ, 216, 610
Volonteri, M., Haardt, F., & Madau, P. 2003, ApJ, 582, 559
Volonteri, M., Lodato, G., & Natarajan, P. 2008, MNRAS, 383, 1079
Volonteri, M., & Natarajan, P. 2009, MNRAS, 400, 1911
Wen, L. 2003, ApJ, 598, 419
Yagi, K., & Seto, N. 2011, PhRvD, 83, 044011
Yang, Y., Bartos, I., Gayathri, V., et al. 2019, PhRvL, 123, 181101
Yu, Q., & Tremaine, S. 2003, ApJ, 599, 1129